View Online / Journal Homepage / Table of Contents for this issue
Dynamic Article Links

Soft Matter

Cite this: *Soft Matter*, 2012, **8**, 9603

www.rsc.org/softmatter

**PAPER**

# Crack-free controlled wrinkling of a bilayer film with a gradient interface†

**Yan Xuan,[a] Xu Guo,[a] Yushuang Cui,[a] Changsheng Yuan,*[a] Haixiong Ge,[a] Bo Cui[b] and Yanfeng Chen[a]**

***Received 1st March 2012, Accepted 6th July 2012***
**DOI: 10.1039/c2sm25487e**

Published on 07 August 2012 on http://pubs.rsc.org | doi:10.1039/C2SM25487E
Downloaded by University of Waterloo on 31 August 2012

We report a crack-free controlled wrinkling method based on a bilayer film system. A liquid UV-curable film is solidified on a uniaxially pre-stretched PDMS elastic sheet by UV-exposure. Subsequently, the sheet is released back to its initial non-stretched state, which results in spontaneous formation of grating wrinkles perpendicular to the stretching direction. An interface of gradient interpenetrating polymer networks (IPN) is considered to be formed between the stiff UV-cured film and the elastic support, which is practically beneficial for preventing crack formation and film delamination during the strain relaxation process. The periodicity of the gratings is tuned by controlling the thickness of the UV-cured polymer film and the amplitude of pre-strain of the elastic sheet. The imprinting results demonstrate that these self-formed wrinkles can serve as a mold to duplicate gratings by nanoimprint lithography. Furthermore, metal gratings are successfully fabricated from the wrinkling molds.

## Introduction

Periodic micro- and submicron-scale gratings have a large variety of significant applications in optoelectronic,[1–4] magnetic,[5] chemical and biological fields.[6,7] Approaches for fabricating patterns are generally classified into two basic types: lithography[8–12] and spontaneous formation (self assembly).[13,14] While lithographic methods offer the advantages of high fidelity and high controllability, e-beam lithography and ion beam lithography have very low throughput and are thus limited to small pattern areas. It is difficult to fabricate small-period gratings using holographic lithography due to the availability of a coherent light source. Nanoimprint lithography, soft lithography and lithographically induced self-construction all require a pre-fabricated mask or mold. As an alternative pathway, there has been a growing interest in the spontaneous formation of periodic micro- and nanostructures. Typical strategies are the self-assembly of amphiphilic lipids, surfactants, block-copolymers or colloidal particles into various patterns and periodicities. Self-assembly is prone to unavoidable defects and has a limited degree of pattern control. Chou *et al.*[15] demonstrated a self-formation method to generate sub-60 nm half-pitch gratings over large areas through fracturing a featureless polymer thin film sandwiched between two flat plates.

Wrinkling is a ubiquitous phenomenon from animal skins to cloth for shrinkage in nature. In the past, wrinkling has been commonly treated as an undesirable failure on surfaces because of its irregularity and uncontrollability. Recently, various methods have been developed to control the formation of wrinkles through thermally or mechanically contracting a two layer system, an elastic sheet capped with a hard coating. In most of the published work, polydimethylsiloxane (PDMS) was used as an elastomeric substrate and a metal film,[16–19] polymer film[20–26] or inorganic/organic film[27] was prepared as an upper hard coating. Highly ordered structures were induced by the buckling of the thin hard film owing to contraction of the underlying substrate. These methods of controlled wrinkling have attracted significant attention due to the applications, including stretchable electronics,[28–32] eyelike digital cameras,[33] cell alignment,[34,35] tunable diffraction and phase grating,[36–38] and measurement of elastic modulus.[39–42] However, on further compression, the wrinkles can evolve to yield folds and cracks depending on the elastic nature of the layered materials. Stone *et al.* elucidated the mechanism of the wrinkle-to-fold transition.[26] The thin films with heterogeneous mechanical properties such as modulus, thickness or stress will also spontaneously curve, roll-up or fold into three dimensional structures such as cylindrical tubes, spirals or polyhedra. These self-assembled or self-folded structures will be further applied in microfluidics, tissue engineering and drug delivery.[43–47]

Since the hard film is intrinsically rather brittle, crack formation parallel to the applied strain is inevitable because of lateral elongation of the elastic substrate[48–50] as the strain is released. In our previous work, we developed a hybrid nanoimprint soft lithography mold, which was composed of a rigid feature layer on an elastic PDMS support.[51] This mold was fabricated by forming a crosslinked polymer pattern layer onto the PDMS

[a]*National Laboratory of Solid State Microstructures, Department of Materials Science and Engineering, College of Engineering and Applied Sciences, Nanjing University, Nanjing, 210093, China. E-mail: csyuan@nju.edu.cn; Fax: +86-25-83621187; Tel: +86-25-83595535*
[b]*Department of Electrical and Computer Engineering, University of Waterloo, 200 University Avenue, West Waterloo, Ontario N2L3G1, Canada*

† Electronic supplementary information (ESI) available. See DOI: 10.1039/c2sm25487e

substrate using a reversal UV-curable imprint process. In this paper, a similar process was applied to solidify a blank film of liquid UV-curable resin on a uniaxially pre-stretched PDMS slab. Subsequently, the strain was removed from the elastic slab and sinusoidal grating wrinkles with a well-defined wavelength were spontaneously generated on the specimen surface perpendicular to the stretching direction. It was considered that an interface of gradient IPN was simultaneously formed between the UV-cured polymer film and elastic support during the solidification of the UV curable film. The gradient interface of IPN effectively prevented crack formation in controlled wrinkling. The self-formed gratings by controlled wrinkling could further serve as a hybrid mold for UV-curable nanoimprint processes and the metal gratings were successfully duplicated on a silicon wafer from the grating hybrid mold.

## Materials and methods

Fig. 1 presents the fabrication procedure of the grating mold by controlled wrinkling. The PDMS elastic sheet was prepared by mixing Sylgard 184 (Dow Corning) in a 10 : 1 mass ratio of base to curing agent, followed by spin-coating on a silicon wafer and curing at 65 °C for 5 h. The thickness of the elastic PDMS sheet (~0.8 mm) was determined by the spin-coating speed of the PDMS prepolymer on the silicon wafer. The PDMS sheet, cut into a 60 mm × 20 mm slab, was clamped onto a custom-built strain stage and pre-stretched as shown in Fig. 2.

The UV-curable material was a home-made UV-curable nanoimprint resist, composed of a low viscosity UV-curable acrylated polydimethylsiloxane material, a multifunctional acrylate cross-linker, and a free radical initiator. Two different processes were used to form a rigid blank polymer film on the pre-stretched PDMS slab. In the first process as shown in Fig. 1a, the liquid UV-curable resist was spin coated on a bare silicon wafer, and then cross-linked and solidified by UV radiation with an exposure of around 300 mJ $cm^{-2}$ in a nitrogen atmosphere. After that, the strain stage with the pre-stretched PDMS slab (Fig. 2a) was placed face down onto the spin-coated wafer. The weight of

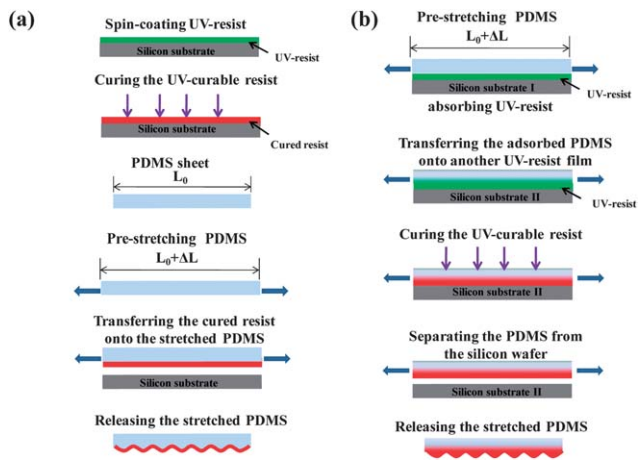


**Fig. 1** Schematic of the process of the controlled wrinkling by two different processes. (a) A cured and solidified resist film transferred onto a pre-stretched PDMS slab and (b) a UV-curable resist film cured and solidified with a pre-stretched PDMS slab.

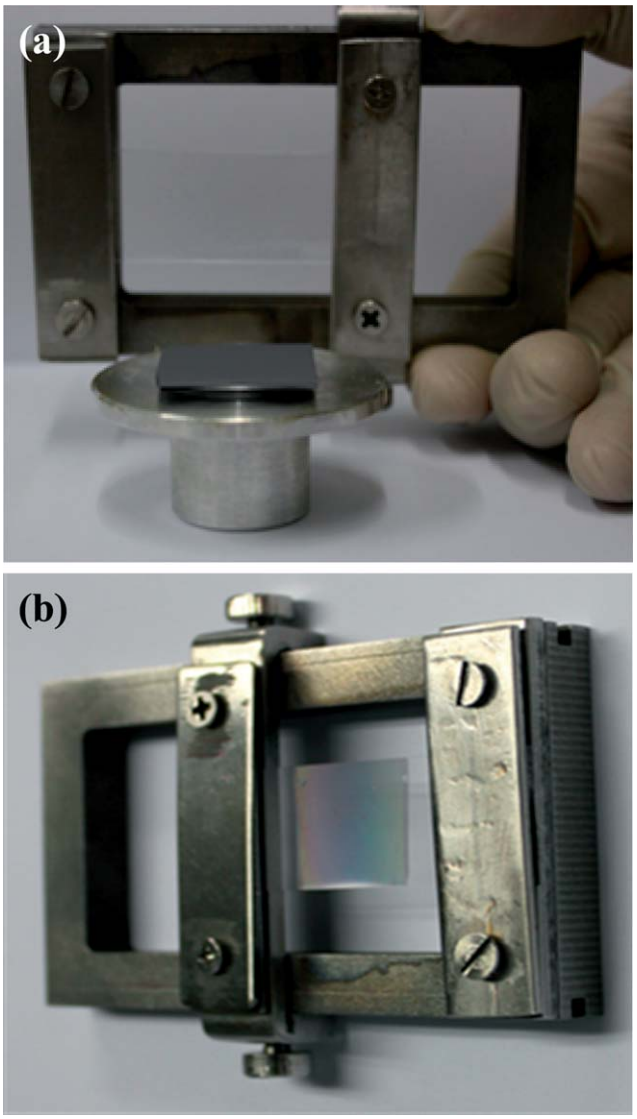


**Fig. 2** Photograph images of (a) placing the pre-stretched PDMS slab on a UV resist film spin-coated on a silicon wafer and (b) a controlled wrinkling sample after the pre-stretched PDMS slab went back to the initial non-stretched state.

strain stage helped bring the stretched PDMS slab into conformal contact with the cross-linked resist film. Subsequently, the stage was removed from the silicon wafer, and then the pre-stretched PDMS slab was allowed to return to its original length by gradually releasing the strain from the PDMS slab. In the second process (Fig. 1b), the stretched PDMS was placed onto a Si wafer, which was pre-coated with a 200 nm thick liquid UV-curable resist film. After 10 minutes, the PDMS slab, absorbed with liquid UV-curable resist, was separated from the Si wafer and then carefully placed onto another spin-coated resist film with an intended thickness. Then, the sample was cured by UV radiation through the transparent PDMS side in a nitrogen atmosphere. After UV-curing, the PDMS slab was separated from the silicon wafer and the strain was gradually released from the PDMS.

The relaxed PDMS slab covered with the resist grating pattern was treated by $O_2$ reactive ion etching (RIE) and then coated

Published on 07 August 2012 on http://pubs.rsc.org | doi:10.1039/C2SM25487E
Downloaded by University of Waterloo on 31 August 2012


This journal is © The Royal Society of Chemistry 2012

with a self-assembled monolayer (SAM) of trichloro(1*H*,1*H*,2*H*,2*H*-perfluorooctyl) silane by vapor phase deposition. This slab was used as a mold to fabricate metal grating patterns through a UV-curing nanoimprint method and lift-off. In the process, the UV-curable nanoimprint resist was spin-coated onto a PMMA film that acted as a lift-off layer and was imprinted by the PDMS slab *via* a hybrid UV-curing nanoimprint soft lithography method. The etching of the silicon-containing resist and PMMA was carried out in a Samco RIE-10R machine. Typical etching recipes were 20 sccm $O_2$, 3.5 mTorr, 50 W power for PMMA and 5 sccm $CHF_3$, 3.5 mTorr, 40 W Power for the cross-linked resist films. A 50 nm thick Au layer was deposited by an e-beam evaporator, and finally a lift-off process was carried out in acetone to remove the PMMA and define the Au grating patterns on the substrate.

## Results and discussion

Fig. 2b shows a representative result after removing the strain from the elongated PDMS substrate covered with a crosslinked polymer film. The iridescent color of diffraction from the surface illustrated that the micro- or submicro-scale periodic structures were formed on the sample over a large area by controlled wrinkling. The wrinkles formed in this system were attributed to the mismatch of elastic moduli between a relatively rigid surface layer with a tensile modulus of 216 N $mm^{-2}$ and a more compliant elastomeric substrate with a tensile modulus of 2.4 N $mm^{-2}$. Upon lateral compression of this system above a certain threshold strain, the planarity of the rigid film was destroyed and periodic wrinkles were formed to minimize the strain energy. In the first preparation process, we directly transferred a 200 nm thick cured polymer film onto a 0.8 mm thick PDMS slab elongated to 30% strain. The quite low surface energy of the cured resist film (water contact-angle measurement of 109°) and the tackiness of the PDMS ensured a complete transfer of the cross-linked polymer film from the silicon wafer onto the elastic slab. Both grating wrinkles and line defects (perpendicular to grating direction) were observed in Fig. 3a and b as the PDMS slab returned to its non-stretched state. These defects were cracks of the cross-linked resist layer during the relaxation process. The cracks were visible by eye. The SEM observation shows that the crack was almost 1 order of magnitude larger than the periodicity of the wrinkles and the delamination occurred at the edge of the cracks. The formation of cracks was mostly attributed to the Poisson effect. The contraction of the stretched PDMS led to a lateral Poisson expansion perpendicular to the contraction direction when the tensile strain was released, which ruptured the brittle cross-linked polymer film.

In the second preparation process, the stretched PDMS was first placed onto a 200 nm thick uncured resist film, which was coated on a Si wafer. After contact for a certain time, the PDMS slab was separated from the Si wafer and then carefully placed onto another uncured resist film. Next, the UV-curing process was carried out in a nitrogen atmosphere because oxygen diffusing through PDMS can inhibit the free radical polymerization of the acrylated resist. After UV-curing, the PDMS slab was removed from the silicon wafer and then the strain was gradually released from the PDMS. No obvious cracks were

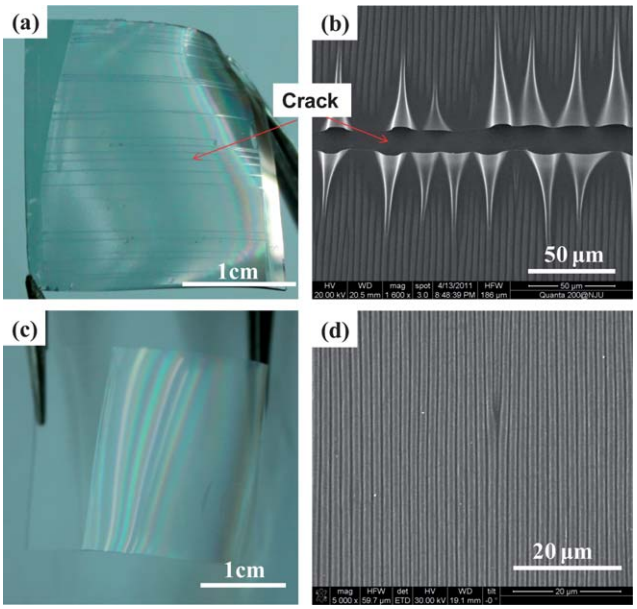


**Fig. 3** Photographs and SEM images of representative controlled wrinkling results formed by two different processes: (a) and (b) are of a cured and solidified resist film transferred onto a pre-stretched PDMS slab; (c) and (d) are a UV-curable resist film cured and solidified onto a pre-stretched PDMS slab.

observed on the wrinkled surface shown in Fig. 3c and d as the PDMS was brought back to the initial non-stretched state. In this case, the preparation process was similar to the sequential polymerization method for the preparation of the gradient IPN. Gradient IPNs are mixtures of cross-linked polymers in which the concentration of one network varies across the section of the matrix.[52–54] They are usually prepared by diffusing a guest monomer or oligomer into a preformed first (host) polymer network for certain periods of time to establish a gradient profile, which is then fixed to form the second (guest) network by polymerization of the diffused monomer *in situ*. Gradient IPNs can be treated as a sequence of an infinite number of layers of IPNs, whose compositions and properties vary gradually from the surface to the core of the material. The cross-linked network of PDMS was found to have an intrinsic high permeability for gases and low molecular weight species, which allowed the low viscosity UV-curable material to be absorbed and diffused inside the matrix of the PDMS. The absorption of the UV-curable material was studied by contact of the PDMS with the UV-curable resist film spin coated on the silicon wafer for various durations. The amount of the absorbed UV resist was determined by the measurement of the thickness of the film that remained on silicon wafer after removing the PDMS. Fig. 4 shows the thickness of the remaining resist at various contact durations. With a fixed initial film thickness, the absorption caused the resist film thickness on the silicon wafer to decrease gradually and significantly over time. For contact times longer than 5 min, the film thickness gradually stabilized and the absorption reached its equilibrium point. Generally, the diffusion may result in a gradient profile of the UV-curable material across the depth of the PDMS sample. During the UV-curing process, the resist on the silicon wafer not only self-polymerized

Published on 07 August 2012 on http://pubs.rsc.org | doi:10.1039/C2SM25487E
Downloaded by University of Waterloo on 31 August 2012

Published on 07 August 2012 on http://pubs.rsc.org | doi:10.1039/C2SM25487E
Downloaded by University of Waterloo on 31 August 2012

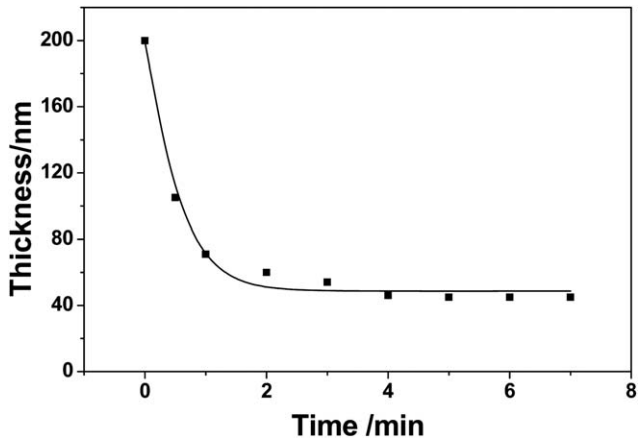


**Fig. 4** Variation of the UV-curable film thickness remaining on the silicon wafer for various contact times of the UV-curable film with the PDMS slab.

but also reacted with the resist molecules, which were diffused into the crosslinked PDMS, and formed a gradient IPN.

In this case, the sample can be divided into three distinct regions, namely, the rigid crosslinked polymer film, a comparatively less rigid interface of gradient IPN near the surface region of the PDMS support and the elastic PDMS. The gradient interface had a gradually changing composition from a rigid cross-linked polymer to an elastomeric structure. It was considered that the elastic modulus at the interface was also varied gradually so that an abrupt stress mismatch could be minimized during wrinkling. It has been proved by previous simulation works[55,56] that incorporation of a graded interlayer between the stiff top coating and elastic substrate can significantly reduce the stress intensity factor of the system, and thus increase the resistance of coatings to functional failure, such as cracking and debonding. In practice, the interface of the gradient IPN was beneficial for preventing crack formation or film delamination of the two-layer system during the controlled wrinkling process. In addition, the IPN provided an excellent bond for the two distinct layers to ensure a complete transfer of the crosslinked polymer film onto the elastic PDMS.

To assess how largely the gradient interface could improve the cracking, we prepared the wrinkling samples with different pre-strain levels and thicknesses of the rigid film. The lateral Poisson contraction orthogonal to the pre-strain direction of the 0.8 mm thick PDMS substrate almost linearly increased from 4% to 35% with increasing the pre-strain from 10% to 100%. The cracks were typically observed on the 400 nm thick rigid film even at a pre-strain of <10% for the wrinkled sample without the gradient interface after the pre-strain relaxation. The sample with the gradient interface (Fig. 5a) did not show any visible cracks at a pre-strain of 10% for the same rigid film thickness.[57] At higher pre-strains than 10%, the films underwent cracking and the crack density was proportional to the applied pre-strain as shown in Fig. 5b–d. These cracks were generated to relieve the strain energy within the thin film as the strain exceeded the critical value. For the thinner film with a thickness of 100 nm (Fig. 5f), no cracks appeared at pre-strains up to 100%. This could be attributed to the fact that the elastic modulus and fracture

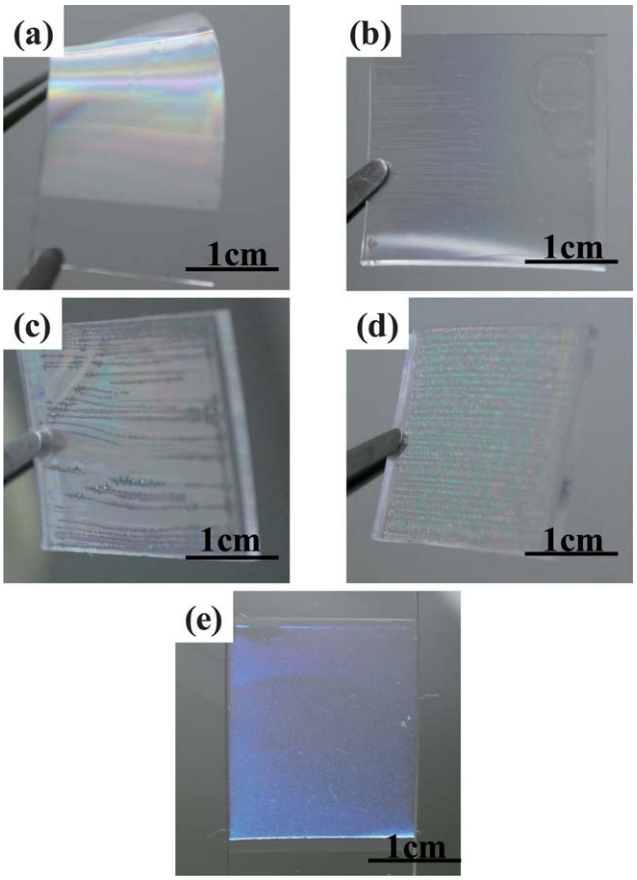


**Fig. 5** Photographs of the wrinkled samples with gradient interfaces with different applied pre-strains and film thickness. (a) 400 nm thickness and 20% pre-strain; (b) 400 nm thickness and 30% pre-strain; (c) 400 nm thickness and 40% pre-strain; (d) 400 nm thickness and 50% pre-strain; (e) 100 nm thickness and 100% pre-strain.

strength of ultrathin polymer films would decrease, but the ductility would increase with a decrease in film thickness. The experimental results indicated that the gradient interface effectively prevented crack formation and film delamination during the strain relaxation process.

The dominant wavelength of the wrinkle patterns can be predicted *via* well-established buckling mechanics according to the following equation:[58]

$$\lambda = \frac{2\pi h_f}{(1+\varepsilon_{pre})(1+\xi)^{1/3}}\left[\frac{E_f\left(1-\nu_s^2\right)}{3E_s\left(1-\nu_f^2\right)}\right]^{1/3} \quad (1)$$

where $\lambda$ is the wavelength of the wrinkle patterns, $h_f$ is the thickness of the upper stiff film, $E$ is the Young's modulus, and $\nu$ is Poisson's ratio. The subscripts "f" and "s" denote stiff film and substrate, respectively. $\xi = 5(1 + \varepsilon_{pre})/32$ represents the large deformation and geometrical non-linearity in the substrate. From the equation, the characteristic periodicity depends on the mechanical properties of the film and substrate as well as the thickness of the rigid film and pre-strain of PDMS. Young's Modulus and Poisson's Ratio are the intrinsic material properties and are fundamentally related to the materials used in the experiment. Thus, the periodicity of the patterns is mainly

 This journal is © The Royal Society of Chemistry 2012

Published on 07 August 2012 on http://pubs.rsc.org | doi:10.1039/C2SM25487E
Downloaded by University of Waterloo on 31 August 2012

determined by two factors: the thickness of the upper stiff film and the pre-strain of the elastic substrate.

In our experiment, the periodicities of the grating wrinkles were tuned by the film thickness of the UV-curable resist and the amplitude of the pre-strain of the PDMS slab. Fig. 6 shows experimental results of controlled wrinkling in the situation of uniaxial strain with various pre-strain levels and a fixed film thickness of 150 nm. The period was obtained from measurement of an average of 5 peak-to-peak distances of parallel grating patterns *via* atomic force microscopy (AFM). Fig. 7b shows a plot of the wavelength as a function of pre-strain as measured from AFM images in Fig. 6a. A three-dimensional AFM perspective view and a cross-sectional profile of 950 nm period wrinkles at a pre-strain of 10% are showed in Fig. 6c and d. The sinusoidal morphology of the wrinkles was clearly observed by AFM, and this profile was further confirmed by the imprint results as shown in Fig. 8a.

The controllable thickness of the crosslinked film was easily obtained by adjusting the thickness of the UV-curable resist film on the silicon wafer through the spin coating process. Fig. 7 shows the controlled wrinkling results with the UV-curable film thickness in the range of 50–400 nm at a pre-strain level of 20%. The wavelength of the wrinkles in Fig. 7a was measured by SEM. It was found that the wrinkles' wavelengths increased from 464 nm to 2500 nm with the increase of the film thickness from 53 nm to 382 nm, and the wavelength was almost linearly proportional to the film thickness of the spin coated resist. The experimental data were generally in good agreement with the theoretical prediction in eqn (1). Compared with the smooth surface of the wrinkling patterns with a stiff film thickness over 382 nm (Fig. 7b), the patterns exhibited a rough and bamboo-like

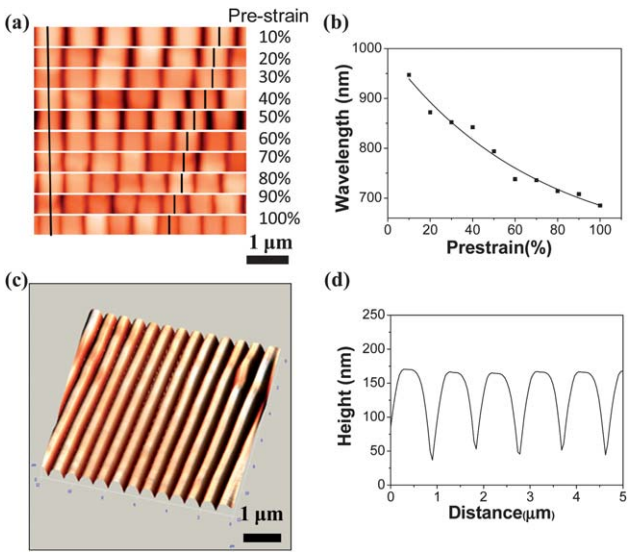


**Fig. 6** The effect of the pre-strain on the wrinkling wavelength for a fixed UV-curable resist film thickness of 150 nm. (a) Plane-view AFM images of controlled wrinkling specimens on PDMS, formed with various pre-strains (indicated on the right in percentage). (b) Profile of wavelength of the controlled wrinkles *vs.* pre-strain as measured from AFM images in (a). (c) Three-dimensional AFM perspective view of a 950 nm period wrinkled pattern formed with a pre-strain of 10%. (d) Line cut profile of the corresponding image in (c).

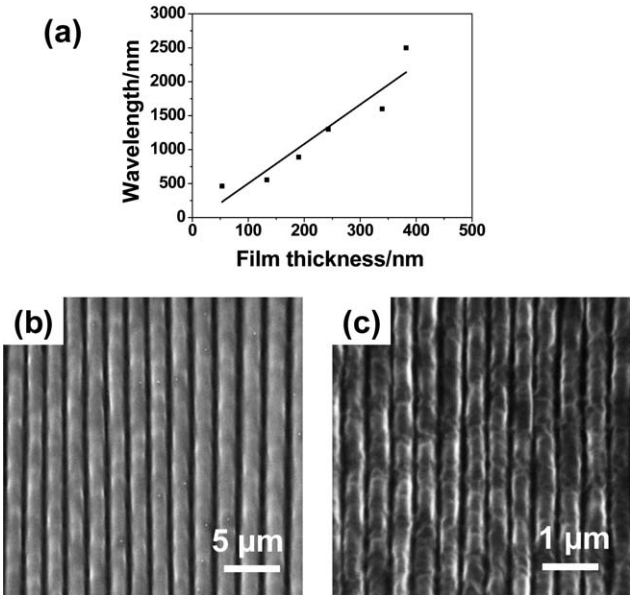


**Fig. 7** The effect of the crosslinked film thickness on the wrinkling wavelength with a fixed pre-strain level of 20%. (a) Profile of wavelength of the controlled wrinkles prepared with different UV-curable film thickness in the range of 50–400 nm as measured by SEM. (b) SEM image of wrinkled patterns formed with the UV-resist film thickness of 382 nm. (c) SEM image of wrinkled patterns formed with the UV-resist film thickness of 53 nm.

surface as the stiff film thickness was decreased to approximately 53 nm (Fig. 7c). No obvious regular wrinkling pattern could be formed when the film thickness was less than 50 nm. This might be because the crosslinked film was so thin that it could not impose sufficient constraint to the contracted PDMS to form regular wrinkles.

Since the cross-linked film was composed of silicon-containing material, the controlled wrinkling specimen could be directly used as a hybrid nanoimprint soft lithography mold after $O_2$ RIE treatment and a coating of fluoroalkyltrichlorosilane release agent. The $O_2$ RIE treatment oxidized the siloxane into silica and formed silanol groups on the wrinkle surface. The fluoroalkyltrichlorosilane release agent was covalently linked to the surface of the cross-linked polymer film by vapor treatment. Fig. 8a

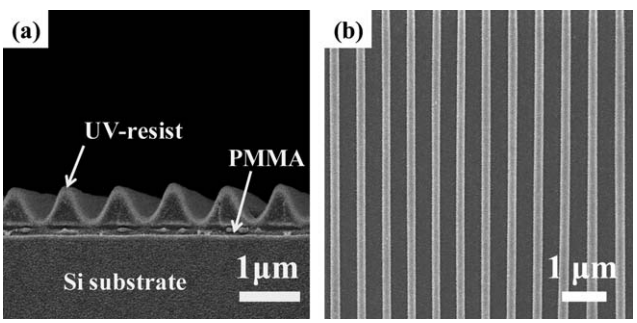


**Fig. 8** (a) A SEM image of sinusoidal grating patterns with a period of 750 nm imprinted on a bilayer UV-curable resist by a controlled wrinkling mold. (b) A SEM image of Au gratings on a silicon wafer fabricated from the corresponding imprinted patterns in (a).

Published on 07 August 2012 on http://pubs.rsc.org | doi:10.1039/C2SM25487E
Downloaded by University of Waterloo on 31 August 2012

shows a SEM image of the grating pattern on the silicon wafer with a period of about 750 nm fabricated *via* a UV-curing imprint process with the wrinkle mold. The imprinted replica represented the negative of the wrinkle mold and reflected the exact geometry of the mold surface. The cross-sectional view of the imprint pattern in fig. 8a displayed a uniform wavy profile, which confirmed the sinusoidal topography of the wrinkle surface observed by AFM. A uniform residual layer of approximately 40 nm thickness indicated that the height of the controlled wrinkling patterns was uniform and the imprinted features could be used for further pattern transfer. Au grating patterns with a 750 nm period (fig. 8b) were successfully duplicated from the wrinkle mold through a double layer resist system, which was composed of the UV-curable resist spin-coated on a PMMA layer for the lift-off process. In the process, the residual layer of imprint resist was removed by fluorine-based RIE, and then the PMMA was etched through by $O_2$ RIE. 50 nm thick Au was deposited on the etched features by e-beam evaporation, and acetone was used as the solvent of PMMA for the lift off process.

## Conclusions

We developed a crack-free, controlled wrinkling method based on a two layer system, an elastic sheet capped with a hard coating. A liquid UV-curable film was solidified on a uniaxially pre-stretched PDMS elastic sheet by UV-exposure and subsequently the strain was released to spontaneously form grating wrinkles perpendicular to the stretching direction. An interface of gradient IPNs was considered to be formed between the stiff UV-cured film and the elastic support. The experimental results indicated that the gradient interface effectively prevented crack formation and film delamination during the strain relaxation process. The periodicity of the gratings could be tuned by adjusting the thickness of the UV-curable film and pre-strain amplitude of the elastic sheet. The self-formed wrinkles could serve as a mold to duplicate the grating patterns by nanoimprint lithography.

## Acknowledgements

This work was jointly supported by the National Nature Science Foundation of China (Grant no. 10874072 and 91023014), the Priority Academic Program Development of Jiangsu Higher Education Institutions and RFDP.

## References

1 C. Kim, M. Shtein and S. R. Forrest, Nanolithography based on patterned metal transfer and its application to organic electronic devices, *Appl. Phys. Lett.*, 2002, **80**, 4051.
2 E. Sakat, G. Vincent, P. Ghenuche, N. Bardou, S. Collin, F. Pardo, J. L. Pelouard and R. Haïdar, Guided mode resonance in subwavelength metallodielectric free-standing grating for bandpass filtering, *Opt. Lett.*, 2011, **36**, 3054.
3 Y. Zhao, Y. Y. Zhang, R. Q. Lv and Q. Wang, Novel optical devices based on the tunable refractive index of magnetic fluid and their characteristics, *J. Magn. Magn. Mater.*, 2011, **323**, 2987.
4 Y. Jourlin, J. Jay, F. Pigeon, G. Bouchet, O. Parriaux, P. van Dijk, R. Pellens, S. Topcu, Y. Alayli and M. Bonis, Wafer scale submicron optical grating for the picometre measurement of aberrations and stitching errors in step and repeat cameras, *Microelectron. Eng.*, 2002, **61–62**, 1101.
5 P. D. Ye, D. Weiss, R. R. Gerhardts, K. Klitzing and S. Tarucha, Huge magnetoresistance oscillations in periodic magnetic fields, *Phys. B*, 1998, **249–251**, 330.
6 B. Cunningham, B. Lin, J. Qiu, P. Li, J. Pepper and B. Hugh, A plastic colorimetric resonant optical biosensor for multiparallel detection of label-free biochemical interactions, *Sens. Actuators, B*, 2002, **85**, 219.
7 P. Vukusic, R. Kelly and I. Hooper, A biological sub-micron thickness optical broadband reflector characterized using both light and microwaves, *J. R. Soc., Interface*, 2009, **6**, 193.
8 S. S. Oh, C. G. Choi and Y. S. Kim, Fabrication of micro-lens arrays with moth-eye antireflective nanostructures using thermal imprinting process, *Microelectron. Eng.*, 2010, **87**, 2328.
9 J. Amako, D. Sawaki and E. Fujii, High-efficiency diffractive beam splitters surface-structured on submicrometer scale using deep-UV interference lithography, *Appl. Opt.*, 2009, **48**, 5105.
10 C. H. Chang, R. K. Heilmann, R. C. Fleming, J. Carter, E. Murphy, M. L. Schattenburg, T. C. Bailey, J. G. Ekerdt, R. D. Frankel and R. Voisin, Fabrication of sawtooth diffraction gratings using nanoimprint lithography, *J. Vac. Sci. Technol., B*, 2003, **21**, 2755.
11 C. Vieu, F. Carcenac, A. Pepin, Y. Chen, M. Mejias, A. Lebib, L. Manin-Ferlazzo, L. Couraud and H. Launois, Electron beam lithography: resolution limits and applications, *Appl. Surf. Sci.*, 2000, **164**, 111.
12 W. Wu, M. Hu, F. Suong Ou, Z. Y. Li and R. S. Williams, Cones fabricated by 3D nanoimprint lithography for highly sensitive surface enhanced Raman spectroscopy, *Nanotechnology*, 2010, **21**, 255502.
13 Y. Anraku, A. Kishimura, M. Oba, Y. Yamasaki and K. Kataoka, Spontaneous formation of nanosized unilamellar polyion complex vesicles with tunable size and properties, *J. Am. Chem. Soc.*, 2010, **132**, 1631.
14 E. Chason and M. J. Aziz, Spontaneous formation of patterns on sputtered surfaces, *Scr. Mater.*, 2003, **49**, 953.
15 S. Y. Chou, P. R. Krauss and P. J. Renstrom, Nanoimprint lithography, *J. Vac. Sci. Technol., B*, 1996, **14**, 4129.
16 G. C. Martin, T. T. Su, I. H. Loh, E. Balizer, S. T. Kowel and P. Kornreich, The metallization of silicone polymers in the rubbery and glassy state, *J. Appl. Phys.*, 1982, **53**, 797.
17 N. Bowden, S. Brittain, A. G. Evans, J. W. Hutchinson and G. M. Whitesides, Spontaneous formation of ordered structures in thin films of metals supported on an elastomeric polymer, *Nature*, 1998, **393**, 146.
18 W. T. S. Huck, N. Bowden, P. Onck, T. Pardoen, J. W. Hutchinson and G. M. Whitesides, Ordering of spontaneously formed buckles on planar surfaces, *Langmuir*, 2000, **16**, 3497.
19 A. L. Volynskii, S. Bazhenov, O. V. Lebedeva and N. F. Bakeev, Mechanical buckling instability of thin coatings deposited on soft polymer substrates, *J. Mater. Sci.*, 2000, **35**, 547.
20 C. M. Stafford, C. Harrison, K. L. Beers, A. Karim, E. J. Amis, M. R. Vanlandingham, H. C. Kim, W. Volksen, R. D. Miller and E. E. Simonyi, A buckling-based metrology for measuring the elastic moduli of polymeric thin films, *Nat. Mater.*, 2004, **3**, 545.
21 D. Mertz, J. Hemmerle, F. Boulmedais, J. C. Voegel, P. Lavalle and P. Schaaf, Polyelectrolyte multilayer films under mechanical stretch, *Soft Matter*, 2007, **3**, 1413.
22 C. Harrison, C. M. Stafford, W. H. Zhang and A. Karim, Sinusoidal phase grating created by a tunably buckled surface, *Appl. Phys. Lett.*, 2004, **85**, 4016.
23 C. H. Lu, I. Donch, M. Nolte and A. Fery, Au nanoparticle-based multilayer ultrathin films with covalently linked nanostructures: spraying layer-by-layer assembly and mechanical property characterization, *Chem. Mater.*, 2006, **18**, 6204.
24 A. J. Nolte, M. F. Rubner and R. E. Cohen, Determining the Young's modulus of polyelectrolyte multilayer films *via* stress-induced mechanical buckling instabilities, *Macromolecules*, 2005, **38**, 5367.
25 A. J. Nolte, R. E. Cohen and M. F. Rubner, A two-plate buckling technique for thin film modulus measurements: applications to polyelectrolyte multilayers, *Macromolecules*, 2006, **39**, 4841.
26 P. Kim, M. Abkarian and H. A. Stone, Hierarchical folding of elastic membranes under biaxial compressive stress, *Nat. Mater.*, 2011, **10**, 925.
27 M. Ouyang, C. Yuan, R. J. Muisener, A. Boulares and J. T. Koberstein, Conversion of some siloxane polymers to silicon oxide by UV/ozone photochemical processes, *Chem. Mater.*, 2000, **12**, 1591.

 This journal is © The Royal Society of Chemistry 2012

View Online

Published on 07 August 2012 on http://pubs.rsc.org | doi:10.1039/C2SM25487E
Downloaded by University of Waterloo on 31 August 2012


28 D. Y. Khang, H. Q. Jiang, Y. Huang and J. A. Rogers, A stretchable form of single-crystal silicon for high-performance electronics on rubber substrates, *Science*, 2006, **311**, 208.
29 C. J. Yu, Z. Y. Wang, H. Y. Yu and H. Q. Jiang, A stretchable temperature sensor based on elastically buckled thin film devices on elastomeric substrates, *Appl. Phys. Lett.*, 2009, **95**, 141912.
30 A. J. Baca, J. H. Ahn, Y. G. Sun, M. A. Meitl, E. Menard, H. S. Kim, W. M. Choi, D. H. Kim, Y. Huang and J. A. Rogers, Semiconductor wires and ribbons for high-performance flexible electronics, *Angew. Chem., Int. Ed.*, 2008, **47**, 5524.
31 J. A. Rogers, T. Someya and Y. G. Huang, Materials and mechanics for stretchable electronics, *Science*, 2010, **327**, 1603.
32 B. Z. Tian, T. Cohen-Karni, Q. Qing, X. J. Duan, P. Xie and C. M. Lieber, Three-dimensional, flexible nanoscale field-effect transistors as localized bioprobes, *Science*, 2010, **329**, 830.
33 W. H. Koo, S. M. Jeong, F. Araoka, K. Ishikawa, S. Nishimura, T. Toyooka and H. Takezoe, Light extraction from organic light-emitting diodes enhanced by spontaneously formed buckles, *Nature*, 2010, **4**, 222.
34 H. C. Ko, M. P. Stoykovich, J. Z. Song, V. Malyarchuk, W. M. Choi, C. J. Yu, J. B. Geddes, J. L. Xiao, S. D. Wang, Y. G. Huang and J. A. Rogers, A hemispherical electronic eye camera based on compressible silicon optoelectronics, *Nature*, 2008, **454**, 748.
35 J. H. Lim, K. S. Lee, J. C. Kim and B. H. Lee, Tunable fiber gratings fabricated in photonic crystal fiber by use of mechanical pressure, *Opt. Lett.*, 2004, **29**, 331.
36 C. W. Wong, P. T. Rakich, S. G. Johnson, M. H. Qi, H. I. Smith, Y. Jeon, G. Barbastathis, S. G. Kim, E. P. Ippen and L. C. Kimerling, Strain-tunable silicon photonic band gap microcavities in optical waveguides, *Appl. Phys. Lett.*, 2004, **84**, 1242.
37 C. M. Stafford, B. D. Vogt, C. Harrison, D. Julthongpiput and R. Huang, Elastic moduli of ultrathin amorphous polymer films, *Macromolecules*, 2006, **39**, 5095.
38 E. A. Wilder, S. Guo, S. Lin-Gibson, M. J. Fasolka and C. M. Stafford, Measuring the modulus of soft polymer networks *via* a buckling-based metrology, *Macromolecules*, 2006, **39**, 4139.
39 D. Tahk, H. H. Lee and D. Y. Khang, Elastic moduli of organic electronic materials by the buckling method, *Macromolecules*, 2009, **42**, 7079.
40 J. Song, H. Jiang, W. M. Choi, D. Y. Khang, Y. Huang and J. A. Rogers, An analytical study of two-dimensional buckling of thin films on compliant substrates, *J. Appl. Phys.*, 2008, **103**, 014303.
41 J. M. Torres, N. Bakken, C. M. Stafford, J. Li and B. D. Vogt, Thickness dependence of the elastic modulus of tris(8-hydroxyquinolinato) aluminium, *Soft Matter*, 2010, **6**, 5783.
42 N. Patrito, C. McCague, P. R. Norton and N. O. Petersen, Spatially controlled cell adhesion *via* micropatterned surface modification of poly (dimethylsiloxane), *Langmuir*, 2007, **23**, 715.
43 H. Vandeparre, S. Gabrele, F. Brau, C. Gay, K. K. Parker and P. Damman, Hierarchical wrinkling patterns, *Soft Matter*, 2010, **6**, 5751.
44 M. Jamal, A. M. Zarafshar and D. H. Gracias, Differentially photo-crosslinked polymers enable self-assembling microfluidics, *Nat. Commun.*, 2011, **2**, 527.
45 L. Ionov, Soft microorigami: self-folding polymer films, *Soft Matter*, 2011, **7**, 6786.
46 B. Yuan, Y. Jin, Y. Sun, D. Wang, J. S. Sun, Z. Wang, W. Zhang and X. Y. Jiang, A strategy for depositing different types of cells in three dimensions to mimic tubular structures in tissues, *Adv. Mater.*, 2012, **24**, 890.
47 R. Fernandes and D. H. Gracias, Self-folding polymeric containers for encapsulation and delivery of drugs, *Adv. Drug Delivery Rev.*, 2012, **12267**, 11.
48 E. Kirill, R. Mindaugas, M. Evangelos, V. Ashkan, L. Mahadevan and G. Jan, Nested self-sinilar wrinkling patterns in skins, *Nat. Mater.*, 2005, **4**, 293.
49 P. Melanie, S. Alexandra, H. Christoph, C. Arnaud, Z. Ute, H. Anne, B. Alexander and F. Andreas, A lithography-free pathway for chemical microstructuring of macromolecules from aqueous solution based on wrinkling, *Langmuir*, 2008, **24**, 12748.
50 F. Huiyang, J. Hanqing and K. Dahl-Young, Nonsinusoidal buckling of thin gold films on elastomeric substrates, *J. Vac. Sci. Technol., A*, 2009, **27**, L9.
51 Z. W. Li, Y. N. Gu, L. Wang, H. X. Ge, W. Wu, Q. F. Xia, C. S. Yuan, Y. F. Chen, B. Cui and R. Stanley Williams, Hybrid nanoimprint soft lithography with sub-15 nm resolution, *Nano Lett.*, 2009, **9**, 2306.
52 Y. S. Lipatov and L. V. Karabanova, Gradient interpenetrating polymer networks, *J. Mater. Sci.*, 1995, **30**, 1095.
53 A. Guneri, Studies with gradient polymers of polystyrene and polymethyl acrylate, *J. Appl. Polym. Sci.*, 1999, **73**, 1721.
54 C. F. Jasso, J. Valdez, J. H. Perez and O. Laguna, Analysis of butyl acrylate diffusion in a glassy polystyrene matrix to predict gradient structure, *J. Appl. Polym. Sci.*, 2001, **80**, 1343.
55 H. J. Choi, Effects of graded layering on the tip behavior of a vertical crack in a substrate under frictional hertzian contact, *Eng. Fract. Mech.*, 2001, **68**, 1033.
56 S. Dag, T. Apatay, M. A. Guler and M. Gulgec, A surface crack in a graded coating subjected to sliding frictional contact, *Eng. Fract. Mech.*, 2012, **80**, 72.
57 J. H. Lee, J. Y. Chung and C. M. Stafford, Effect of confinement on stiffness and fracture of thin amorphous polymer, *ACS Macro Lett.*, 2012, **1**, 122.
58 H. Q. Jiang, D. Y. Khang, J. Z. Song, Y. G. Sun, Y. G. Huang and J. A. Rogers, Finite deformation mechanics in buckled thin films on compliant supports, *Proc. Natl. Acad. Sci. U. S. A.*, 2007, **104**, 15607.